Energy Proceedings
Vol 38, 2024
ISSN 2004-2965

An adaptive internal state observer based on the cubature Kalman filter algorithm for a vehicular PEMFC system

Hongwei Yue[1], Hongwen He[1*], Xuyang Zhao[1], Mo Han[1]

1 National Engineering Laboratory for Electric Vehicles, Beijing Institute of Technology, Beijing, China;

(*Corresponding Author: hwhebit@bit.edu.cn)

ABSTRACT

Ensuring a timely and appropriate supply of reactants is paramount for optimizing fuel cell performance. However, achieving precise reactant control depends on accurately determining the system's internal state. In this paper, the challenge of directly measuring the internal state of vehicular PEMFCs is addressed by proposing an adaptive internal state observer. Firstly, an air subsystem model with five state variables is established based on experimental data. This model effectively describes the critical dynamic features of air flow in the fuel cell system. Secondly, a cubature Kalman filtering algorithm is used to estimate the internal state of the cathode side of the PEMFC. To improve the algorithm's flexibility and minimize estimation errors caused by variations of model parameters, a forgetting factor is introduced, which dynamically adjusts the algorithm's parameters based on the changing conditions of the model. Finally, the simulation comparison demonstrates that the ACKF effectively mitigates the degradation of estimation accuracy with strong robustness as the variation of key structural parameters increases. The ACKF reduces the IAE to 15.05% and 10.92% of the CKF when the selected structural parameters vary by 5%, and to 9.82% and 4.87% respectively when the variation is 10%.

Keywords: proton exchange membrane fuel cell, oxygen excess ratio, cubature Kalman filter, forgetting factor

NONMENCLATURE

Abbreviations	
PEMFC	Proton Exchange Membrane Fuel Cell
OER	Oxygen Excess Ratio
EKF	Extended Kalman filter
UKF	Unscented Kalman filter
CKF	Cubature Kalman filter
ACKF	Adaptive cubature Kalman filter
IAE	Integral of absolute errors
ISE	Integral of squared errors

1. INTRODUCTION

In the context of carbon neutral policy, new energy vehicles have gained unprecedented rapid progress[1], among which, proton exchange membrane fuel cell (PEMFC) vehicles have gained remarkable attention for their clean and efficient characteristics. The supply of reactants has a direct influence on the output characteristics of PEMFC[2–4]. If the supply of reactants is too low, it will easily lead to difficulty in responding to the changing load demand, which reduces the dynamic performance of the vehicle, the so-called reactant starvation phenomenon[5]; if there are too many reactants, it will increase the parasitic power of the PEMFC and reduce the overall efficiency.

Compared to the hydrogen supply system, the air supply system, in which air is delivered into the cathode of the stack by an air compressor, has a much slower response time and is therefore more difficult to control. The air supply is indicated by the oxygen excess ratio (OER), defined as the ratio of the oxygen flow into the cathode and the oxygen in demand for the electrochemical reaction[6][7]. However, the calculation of the OER requires an accurate gas state internal to the cathode, which is difficult to obtain using sensors in actual systems[8]. Therefore, sensorless estimation algorithms become an effective solution to this problem.

With the significant advantage of being able to achieve optimal state estimation, the Kalman filter is one of the most widely used observation algorithms in industry at present. The extended Kalman filter (EKF) achieves local linearization of nonlinear functions using Jacobi matrices on the basis of the basic KF, thus making the application of Kalman filter on nonlinear systems possible. Ma et al.[9] used EKF to obtain predictive parameters and thus predict the aging trend of the fuel cell. The unscented Kalman filter (UKF) solves the nonlinear transfer problem of mean and covariance based on the idea of approximating the probability density distribution of a nonlinear function, which avoids

This is a paper for 15th International Conference on Applied Energy (ICAE2023), Dec. 3-7, 2023, Doha, Qatar.

the additionally introduced linearization error. Chen et al. [10]verified that UKF can estimate PEMFC's working state with high accuracy, and can improve PEMFC's economy in combination with energy management strategies. Some new Kalman filters are developed as well, such as the cubature Kalman filter combined with the spherical rule and the radial rule utilizing a set of equally weighted cubature points to approximate a Bayesian probability distribution. Yuan et al. [11] compared the estimation effect of UKF and CKF on PEMFC cathode state and concluded that CKF has higher accuracy and robustness.

However, current related studies usually do not focus on the effect of system structural parameters. As the service life accumulates, the structural parameters of the PEMFC will gradually develop deviations from the nominal values, which will further increase the inconsistency between the model and the system, thus weakening the observational performance of the observer. In this paper, an adaptive CKF combined with a forgetting factor is proposed based on the judgment of structural parameter changes to cope with the challenge of model inconsistency.

This paper is organized as follows: Section 2 introduces the nonlinear dynamic model of the air supply system and describes the main characters of the key components. Section 3 introduces the judgment conditions of model structure changes, and the adaptive CKF observer based on forgetting factor under the condition of model changes is proposed. In Section 4 the estimation performance of ACKF under nominal structure parameters is verified, and the robustness of ACKF and traditional CKF is compared under the scenario of structure change. And the main contributions of this paper are summarized in Section 5.

2. DYNAMIC MODELLING OF AIR SUBSYSTEM

2.1 Model description

The proton exchange membrane fuel cell (PEMFC) displays highly coupled, nonlinear characteristics and comprises various system components illustrated in Fig. 1. Among them, the air supply system plays the role of supplying the appropriate amount of air to maintain the load demand. Accordingly, in this section, to emphasize key attributes of the PEMFC while taking into account computational demands, this paper constructs a fifth-order nonlinear dynamic model of the PEMFC with the air compressor speed, supply manifold pressure, oxygen and nitrogen partial pressures inside the cathode, and exhaust manifold pressure as state variables.

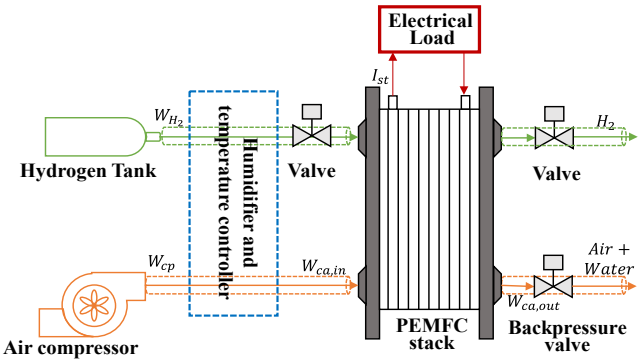

Fig. 1. PEMFC schematic diagram

2.1.1 Air compressor

The air compressor transfers external air into the air subsystem and adjusts the air flow rate according to the operating conditions, and its mechanical angular velocity ω_{cp} is calculated from the input torque τ_{cm} and the load torque τ_{cp}, as shown in Eq. (1).

$$\frac{d\omega_{cp}}{dt} = \frac{1}{J_{cp}}(\tau_{cm} - \tau_{cp}) \tag{1}$$

where J_{cp} is the combined compressor motor inertia. τ_{cm} and τ_{cp} are obtained from Eq. (2).

$$\begin{cases} \tau_{cm} = \dfrac{\eta_{cm} K_t}{R_{cm}}(u_{cp} - K_v \omega_{cp}) \\ \tau_{cp} = \dfrac{C_p T_{atm}}{\eta_{cp}\omega_{cp}}\left[\left(\dfrac{p_{sm}}{p_{atm}}\right)^{\frac{\gamma-1}{\gamma}} - 1\right] W_{cp} \end{cases} \tag{2}$$

where u_{cp} is the input voltage; K_t, R_{cm} and K_v are the motor constants; η_{cm} and η_{cp} are the mechanical efficiency and the compressor efficiency; C_p is the specific heat capacity of air; p_{sm} and p_{atm} are the pressure of supply manifold and atmosphere; T_{atm} is the atmosphere temperature; γ is the specific heats ratio of air. The air flow output from the compressor W_{cp} is fitted as a polynomial function of ω_{cp} and pressure ratio P_r based on the experimental data, as shown in Fig. 2.

$$W_{cp} = a_{00} + a_{10}\omega_{cp} + a_{20}\omega^2 + a_{01}P_r + a_{02}P_r^2 + a_{11}\omega_{cp}P_r \tag{3}$$

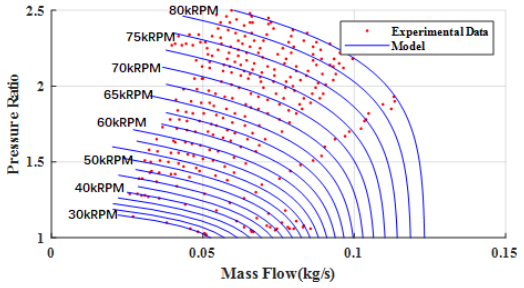

Fig. 2. Air compressor output performance

2.1.2 Manifold system

The manifold system is used to transfer air to the cathode and exhaust it out of the air subsystem, which includes a supply manifold and an exhaust manifold, whose kinetic equations are shown in Eq. (4).

$$\begin{cases} \dfrac{dp_{sm}}{dt} = \dfrac{\gamma R_a T_{cp}}{V_{sm}}\left(W_{cp} - W_{sm,out}\right) \\ \dfrac{dp_{rm}}{dt} = \dfrac{R_a T_{st}}{V_{rm}}\left(W_{ca,out} - W_{rm,out}\right) \end{cases} \tag{4}$$

where p_{sm}, p_{rm}, V_{sm}, V_{rm} are the pressure and the temperature of the supply manifold and the exhaust manifold; T_{st} is the temperature of stack which equals 353 K; T_{cp} is the temperature of air compressor; $W_{sm,out}$, $W_{ca,out}$ and $W_{rm,out}$ are the mass flow of the supply manifold outlet, the stack manifold outlet and the exhaust manifold outlet.

2.1.3 Cathode flow model

Hydrogen ions react electrochemically with oxygen at the PEMFC cathode, and the dynamic equation for the cathodic side, assuming saturated water vapor, is shown in Eq. (5).

$$\begin{cases} \dfrac{dm_{O_2}}{dt} = W_{O_2,in} - W_{O_2,out} - W_{O_2,rct} \\ \dfrac{dm_{N_2}}{dt} = W_{N_2,in} - W_{N_2,out} \end{cases} \tag{5}$$

where m_{O_2}, m_{N_2} represent the mass of the oxygen, nitrogen in the cathode; $W_{O_2,in}$, $W_{N_2,in}$, $W_{O_2,out}$, $W_{N_2,out}$ are respectively the mass flow rates of oxygen and nitrogen into and out of the cathode; $W_{O_2,rct}$ is the mass flow of oxygen consuming in the reaction, which can be calculated as Eq. (6).

$$W_{O_2,rct} = M_{O_2}\frac{nI_{st}}{4F} \tag{6}$$

where M_{O_2} is the molar mass of oxygen; n is the number of cells in the stack; I_{st} is the demanded current; F is the Faraday constant.

The details of the dynamic model can be found in Ref.[12]; this paper will not elaborate further.

2.2 Problem statement

From the above analysis, it is evident that the nonlinear relationship between the different components of the air supply system can be represented as a differential equation, as illustrated in Eq. (7).

$$\begin{cases} \dot{x} = F(x) + G \cdot u + D \cdot d \\ y = H(x) \end{cases} \tag{7}$$

where $x = [x_1, x_2, x_3, x_4, x_5]^T = \left[\omega_{cp}, p_{sm}, m_{O_2}, m_{N_2}, p_{rm}\right]^T \in \Re^5$ is the system states vector; the $F(x) \in \Re^5$ represents the nonlinear dynamic process of the system; the $y = [x_1, x_2, x_5]^T \in \Re^3$ represents the system status that can be measured by the sensor and provided to CKF; $u = u_{cp}$ is the operation variable and $d = I_{st}$ is the measurable disturbance.

3. ADAPTIVE CKF OBSERVER

3.1 Cubature Kalman filter

The significant advantage of the CKF algorithm over the EKF is that it does not rely on Jacobi matrices and therefore is not restricted to the form of nonlinear functions, making it particularly suitable for applications to complex high-dimensional systems. Meanwhile, for fifth-order systems, CKF shows greater advantages than UKF in terms of filtering accuracy and numerical stability.

The recursive formulation of the Bayesian filtering algorithm has the expression form shown in Eq. (8).

$$I(f) = \int f(x)\exp(-x^T x)\,dx \tag{8}$$

where $\exp(-x^T x)$ represents the Gaussian density function.

The CKF algorithm transforms Eq. (8) into Spherical-Radial form, let $x = rz$ and $z^T z = 1$, then $x^T x = r^2$. Eq. (8) can be rewritten in the form of Eq. (9).

$$I(f) = \int_0^{\infty}\int_{U_n} f(rz) r^{n-1}\exp(-r^2)\,d\sigma(z)dr \tag{9}$$

where U_n is the surface of an n-dimensional sphere; and $\sigma(\cdot)$ represents the spherical metric.

Combining the third-order spherical rule and the radial rule, the numerical calculation of Eq. 9 is shown in Eq. (10).

$$I(f) \approx \sum_{i=1}^{m}\omega^{(i)} f(\xi_i) \tag{10}$$

where m is the number of the cubature points; $\omega^{(i)} = \frac{1}{m}$ is the weighting coefficients; the ξ_i is the cubature points. For a more detailed derivation of the procedure refer to Ref.[13].

The main process of CKF algorithm includes the following four steps：

Step1: Initialize the state and covariance：

$$\hat{x}_0^+ = E(x_0) \tag{11 a}$$

$$P_0^+ = E[(x_0 - \hat{x}_0)(x_0 - \hat{x}_0)^T] \tag{11 b}$$

Step2: Calculate cubature points and update state and covariance prior estimate:

$$\chi_{k|k}^{(i)} = \hat{x}_k^+ + U_k\sqrt{S_k}\xi_i \tag{12 a}$$

$$x_{k+1|k}^{(i)} = F\left(\chi_{k|k}^{(i)}, u_k, I_k\right) \tag{12 b}$$

$$\hat{x}_{k+1}^- = \sum_{i=1}^{2n}\omega^{(i)} x_{k+1|k}^{(i)} \tag{12 c}$$

$$P_{k+1}^{-}=\sum_{i=1}^{2n}\omega^{(i)}\left(x_{k+1|k}^{(i)}-\hat{x}_{k+1}^{-}\right)\left(x_{k+1|k}^{(i)}-\hat{x}_{k+1}^{-}\right)^{T}+Q_k \quad (12\,d)$$

Step3: Calculate the cubature points of the output equation and update the covariance and cross-covariance:

$$\chi_{k+1|k}^{(i)}=\hat{x}_{k+1}^{-}+U_{k+1}^{-}\sqrt{S_{k+1}^{-}}\xi_i \quad (13\,a)$$

$$y_{k+1|k}^{(i)}=H\left(\chi_{k+1|k}^{(i)}\right) \quad (13\,b)$$

$$\hat{y}_{k+1}^{-}=\sum_{i=1}^{2n}\omega^{(i)}\cdot y_{k+1|k}^{(i)} \quad (13\,c)$$

$$P_{yy,k+1}=\sum_{i=1}^{2n}\omega^{(i)}\left(y_{k+1|k}^{(i)}-\hat{y}_{k+1}^{-}\right)\left(y_{k+1|k}^{(i)}-\hat{y}_{k+1}^{-}\right)^{T}+R_k \quad (13\,d)$$

$$P_{xy,k+1}=\sum_{i=1}^{2n}\omega^{(i)}\left(x_{k+1|k}^{(i)}-\hat{x}_{k+1}^{-}\right)\left(y_{k+1|k}^{(i)}-\hat{y}_{k+1}^{-}\right)^{T} \quad (13\,e)$$

Step4: Calculate the Kalman gain and the posterior estimate:

$$K_{k+1}=P_{xy,k+1}\cdot P_{yy,k+1}^{-1} \quad (14\,a)$$

$$\hat{x}_{k+1}^{+}=\hat{x}_{k+1}^{-}+K_{k+1}(y_{k+1}-\hat{y}_{k+1}^{-}) \quad (14\,b)$$

$$P_{k+1}^{+}=P_{k+1}^{-}-K_{k+1}P_{yy,k+1}K_{k+1}^{T} \quad (14\,c)$$

where Q_k and R_k are the noise variance; S_k and U_k are the diagonal and orthogonal matrices for SVD decomposition of covariance P_k^{+}.

3.2 Adaptive process

Considering the influence of environmental factors and cumulative service time, the structural parameters of PEMFC will change to some extent, and the traditional CKF method is difficult to maintain its estimation accuracy in the case of time-varying structural parameters. Therefore, it is necessary to introduce an adaptive process to ensure the estimation performance of the algorithm by adjusting the algorithm parameters in real time.

The change of actual structural parameters will cause a significant increase in the observation error ε in CKF. Therefore, a judgement parameter δ based on the ε and covariance P_{yy} can be constructed to determine whether the structural parameter shift has occurred, as shown in Eq. (15). When δ is greater than the set value δ_0, it can be considered that the model parameters have changed.

$$\delta_k=\varepsilon_k^{T}\left(P_{yy,k}\right)^{-1}\varepsilon_k \quad (15)$$

where $\varepsilon_k=y_k-\hat{y}_k^{-}$.

The adaptive process consists of two parts: the judgment process and the introduction of forgetting factor. The complete logic of adaptive CKF algorithm is shown in Fig. 3.

Step5: Update noise variance:

$$L_{k+1}=\sum_{i=1}^{2n}\omega^{(i)}\left(y_{k+1|k}^{(i)}-\hat{y}_{k+1}^{-}\right)\left(y_{k+1|k}^{(i)}-\hat{y}_{k+1}^{-}\right)^{T} \quad (16\,a)$$

$$R_{k+1}=\alpha R_k+(1-\alpha)\left(\varepsilon_k\varepsilon_k^{T}+L_{k+1}\right) \quad (16\,b)$$

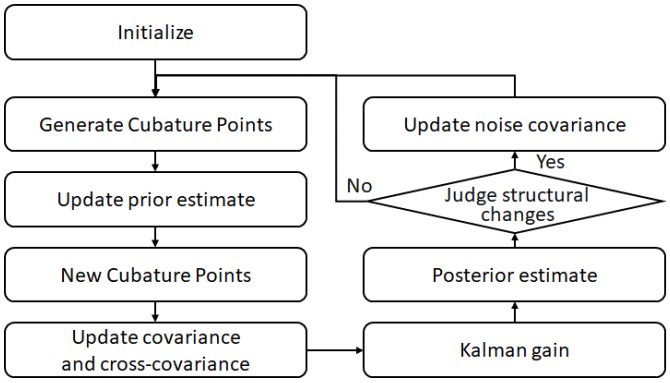

Fig. 3. Logic diagram of the adaptive CKF algorithm

4. RESULTS AND DISCUSSION

4.1 Estimation effect

To verify the estimation effect of the proposed observer, a simulation scenario is set up as shown in Fig. 4. The scenario involves loading and unloading of the OER reference and load current, and the effect of current disturbance is taken into account while evaluating the estimation capability of the observer for OER. In this paper, the conventional CKF is used as a comparison algorithm to show the outstanding superiority of the improved content. The gas state within the cathode cannot be measured in the actual system. To assess the performance of ACKF observation, the PEMFC state variables are calculated analytically in the simulation model, which provides the estimation error of the observer. Fig. 5 shows the estimation of the oxygen and

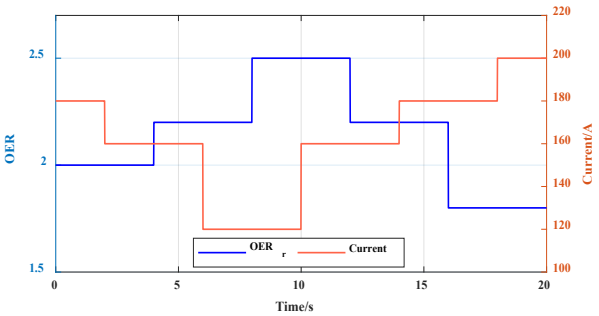

Fig. 4. OER setpoints and load current

nitrogen mass inside the cathode and the OER values reconstructed by both observers.

As shown in Fig. 5, when the structural parameters of the system are nominal values, the estimation effects of ACKF and CKF are approximate, and both are able to close the real value of the system. In terms of the reconstructed OER, the integral of absolute errors (IAE) of ACKF and CKF are 0.0969 and 0.1111, respectively, and the integral of squared errors (ISE) are 0.0011 and 0.0023, which shows that the estimation effect of ACKF is slightly better than that of CKF. In terms of estimating the mass of oxygen and nitrogen, the results of ACKF and CKF are basically the same, and the IAE and ISE of oxygen estimation are 3.198×10^{-5}, 1.027×10^{-4} and 8.925×10^{-11}, 1.060×10^{-9}, respectively. The IAE and ISE for nitrogen are 3.044×10^{-5}, 4.448×10^{-5}, and 7.748×10^{-11}, 2.304×10^{-10} respectively.

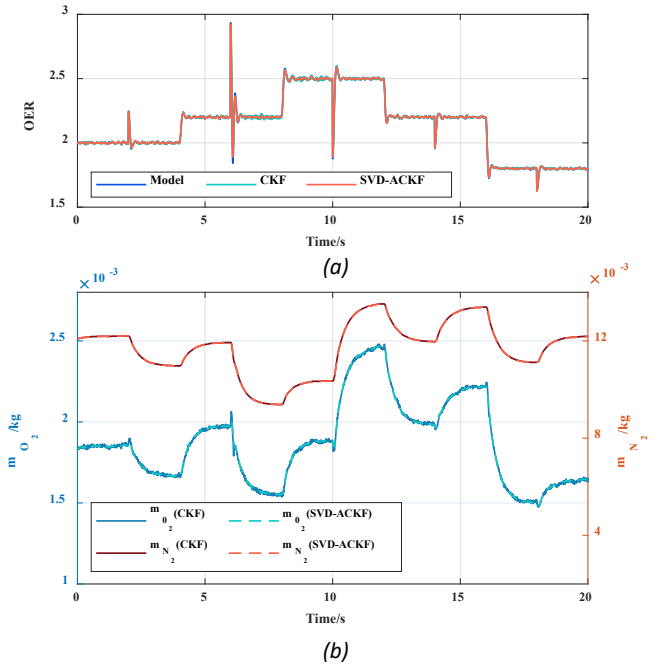

Fig. 5. Estimation of OER, oxygen and nitrogen

Meanwhile, from Fig. 5(a), the variation of load current has a greater impact than the step change of OER setpoints. At the 6th and 10th seconds, the current change is 40A, and the OER of the system shows a large fluctuation, which is caused by the definition of OER. The load current affects the oxygen mass consumed at the cathode, thus leading to sudden changes in the OER values.

4.2 Robust performance

The structural parameters have a great influence on the operation of the actual system. To verify the estimation effect of the proposed ACKF in the case of changing structural parameters, this paper takes the flow factor k_{sm} and k_{rm}, which are used to calculate the gas flow into and out of the cathode, as the structural parameter to be adjusted, and sets them to 1, 0.95 and 0.9, respectively, and compares the estimation effects of the traditional CKF and ACKF. The formula associated with k_{sm} and k_{rm} is shown in Eq. (17). Fig. 6 shows the estimation performance of the two observers with different result parameters.

$$\begin{cases} W_{sm,out} = k_{sm}(p_{sm} - p_{ca}) \\ W_{ca,out} = k_{rm}(p_{ca} - p_{rm}) \end{cases} \tag{17}$$

where p_{sm}, p_{ca} and p_{rm} are pressure in supply manifold, cathode and exhaust manifold, respectively.

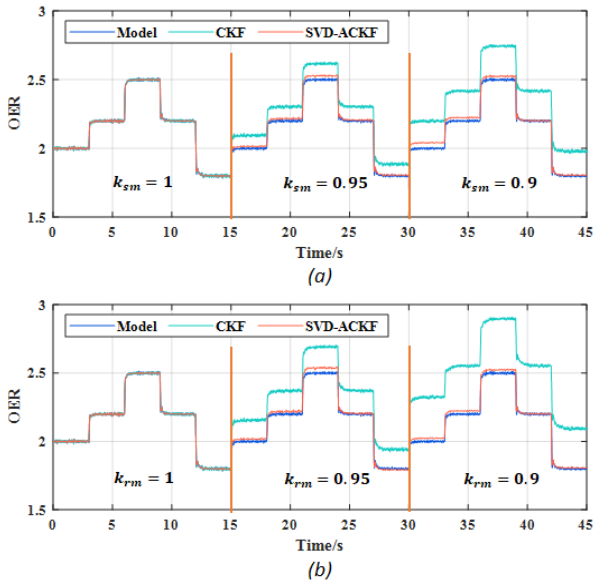

Fig. 6. Robust to structural parameters

It can be intuitively judged from Fig. 6 that when k_{sm} and k_{rm} change, CKF has a significant estimation deviation, and the deviation caused by k_{rm} is more obvious under the same variation amplitude. The ACKF can follow the true value of the system with a smaller error. The errors under different structural parameters are shown in Table 1.

Table 1. Errors for different structural parameters

Structural parameter	IAE		ISE	
	CKF	ACKF	CKF	ACKF
Nominal value	0.0753	0.0593	8.5366×10^{-4}	4.7437×10^{-4}
$k_{sm}=0.95$	1.5110	0.2274	0.1545	0.0050
$k_{sm}=0.9$	3.1718	0.3116	0.6782	0.0100
$k_{rm}=0.95$	2.4874	0.2715	0.4175	0.0072
$k_{sm}=0.9$	5.1684	0.2519	1.7987	0.0059

The model differences caused by the structural parameters can be more intuitively seen through the judgment parameters. Taking the variation of k_{sm} as an example, the determination parameters of traditional CKF and ACKF when k_{sm} takes different values are shown in Fig. 7. It is obvious that when the variation of k_{sm} is larger, the increase of the judgment parameters in the CKF algorithm is more significant. In the ACKF algorithm, due to the existence of adaptive process, the difference of the model is corrected in time, so the value of the judgment parameter is limited to the specified range.

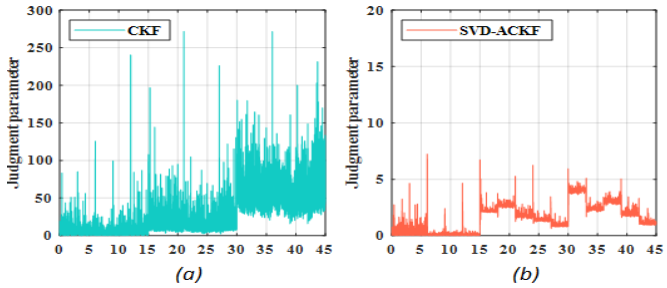

Fig. 7. Judgment parameter of different observers

5. CONCLUSIONS

In this paper, a fifth-order nonlinear dynamic model of air subsystem is established based on bench test data, and an adaptive CKF based on model judgment is proposed. The judgment parameter is used to determine whether the model structure has changed, and the forgetting factor is introduced to adjust the CKF parameters to eliminate the inconsistency of the model. Simulation comparison shows that ACKF has slightly better estimation performance than traditional CKF under nominal structural parameters, and excellent robustness under varying structural parameters, making IAE lower than 0.5 under different structural parameters.

ACKNOWLEDGEMENT

This work was supported by the National Key Research and Development Program of China (No. 2022YFB2502505).

REFERENCE

[1] Zhao X, He H, Li J, Wei Z, Huang R, Shi M. From grayscale image to battery aging awareness—a new battery capacity estimation model with computer vision approach. IEEE Trans Ind Informatics 2022;19:8965–75. https://doi.org/10.1109/TII.2022.3216904.

[2] Ma Y, Zhang F, Gao J, Chen H, Shen T. Oxygen excess ratio control of PEM fuel cells using observer-based nonlinear triple-step controller. Int J Hydrogen Energy 2020;45:29705–17. https://doi.org/10.1016/j.ijhydene.2019.10.089.

[3] Li J, Yu T. A new adaptive controller based on distributed deep reinforcement learning for PEMFC air supply system. Energy Reports 2021;7:1267–79. https://doi.org/10.1016/j.egyr.2021.02.043.

[4] Li J, Yu T, Yang B. Coordinated control of gas supply system in PEMFC based on multi-agent deep reinforcement learning. Int J Hydrogen Energy 2021;46:33899–914. https://doi.org/10.1016/j.ijhydene.2021.07.009.

[5] Wang Y, Wang Y, Zhao J, Xu J. Observer-based adaptive neural network control for PEMFC air-feed subsystem. Appl Soft Comput 2021;113:108003. https://doi.org/10.1016/j.asoc.2021.108003.

[6] Yang D, Pan R, Wang Y, Chen Z. Modeling and control of PEMFC air supply system based on T-S fuzzy theory and predictive control. Energy 2019;188:116078. https://doi.org/10.1016/j.energy.2019.116078.

[7] Chen H, Liu B, Zhang T, Pei P. Influencing sensitivities of critical operating parameters on PEMFC output performance and gas distribution quality under different electrical load conditions. Appl Energy 2019;255:113849. https://doi.org/10.1016/j.apenergy.2019.113849.

[8] Yuan H, Dai H, Ming P, Zhan J, Wang X, Wei X. A fuzzy extend state observer-based cascade decoupling controller of air supply for vehicular fuel cell system. Energy Convers Manag 2021;236:114080. https://doi.org/10.1016/j.enconman.2021.114080.

[9] Ma R, Xie R, Xu L, Huangfu Y, Li Y. A Hybrid Prognostic Method for PEMFC with Aging Parameter Prediction. IEEE Trans Transp Electrif 2021;7:2318–31. https://doi.org/10.1109/TTE.2021.3075531.

[10] Chen K, Laghrouche S, Djerdir A. Performance analysis of PEM fuel cell in mobile application under real traffic and environmental conditions. Energy Convers Manag 2021;227:113602. https://doi.org/10.1016/j.enconman.2020.113602.

[11] Yuan H, Dai H, Wei X, Ming P. A novel model-based internal state observer of a fuel cell system for electric vehicles using improved Kalman filter approach. Appl Energy 2020;268:115009. https://doi.org/10.1016/j.apenergy.2020.115009.

[12] Sun L, Shen J, Hua Q, Lee KY. Data-driven oxygen excess ratio control for proton exchange membrane fuel cell. Appl Energy 2018;231:866–75. https://doi.org/10.1016/j.apenergy.2018.09.036.

[13] Fu H, Cheng Y, Cheng C. A novel improved cubature Kalman filter with adaptive generation of cubature points and weights for target tracking. Meas Sci Technol 2022;33. https://doi.org/10.1088/1361-6501/ac3785.